24th EUROPEAN ROTORCRAFT FORUM
Marseilles, France - 15th-17th September 1998

AC08

Realtime BVI Noise Identification from Blade Pressure Data

Heiko Honert, Berend G. van der Wall,
DLR Institute for Flight Mechanics, Braunschweig, Germany
M. Fritzsche, Daimler Benz, Ulm, Germany
G. Niesl, Eurocopter Deutschland, Donauwoerth, Germany

This paper presents the development and validation of 3 algorithms for the identification and quantification of the actually radiated BVI noise of a helicopter rotor in flight. The main principles of the signal processing for the algorithms handling the data in the time domain, in the frequency domain and by continuous wavelet transforms will be described. A validation of the analysis methods will be given, using wind tunnel data. Finally some results of IBC flight tests will be shown. Besides the description of the flight condition analysis, the single time history output of the different BVI analysis methods from the flight tests will be compared with the data from microphones, which were mounted at the fuselage of the helicopter. The noise measurements on ground for the phase variation of the $2/rev$ IBC input will be refered to the mean values of the BVI analysis outputs. After all the results of rotor simulations will be related to the flight test data.

Nomenclature

Abbreviations

BL	Baseline
BVI	Blade Vortex Interaction
DLR	Deutsches Zentrum fuer Luft- und Raumfahrt
ECD	Eurocopter Deutschland
FFT	Fast Fourier Transform
FWH	Ffowcs-Williams/Hawkings
HART	HHC Aeroacoustic Rotor Test
HHC	Higher Harmonic Control
IBC	Individual Blade Control
MFLOPS	Mega Floating Point Operations/s
MN	Minimum Noise
MV	Minimum Vibration
ZFL	ZF-Luftfahrttechnik

Symbols

a	wavelet scaling factor
$a_i,\ b_i$	Fourier coefficients
c	airfoil chord, m
c_0	speed of sound, m/s
C_n	normal force coefficient
C_T	thrust coefficient
CWT	Continuous Wavelet Transforms
f	frequency, Hz
i	sampling location
I_I	intrusion index
l_r	force on the fluid per unit area in observer direction, N/m^2
L_{mid}	mid-frequency noise level, dB
LA	A weighted noise level, dB
m	helicopter weight, kg
M	Mach number
M_r	rel. Mach number (source $\rightarrow$ observer)
N	number of blades
N_P	number of pressure transducers
N_i	number of samples
p	sound pressure, Pa
P	blade pressure, kPa
QC	quality criterion
$r,\ R$	radial coordinate, rotor radius, m
S	blade surface, m^2

t	time, s
T	time period, s
V	airspeed of the helicopter, m/s
v_n	blade normal velocity disturbance
w	wavelet function
W	weighting function
$x,\ y,\ z$	kartesian coordinates, m
α	angle of attack, deg
β_{1C}	tip path plane tilt angle in pitch direction, deg
β_{BVI}	angle between leading edge and vortex axis, deg
ϵ	shaft tilt angle, deg
γ	flight path angle, deg
μ	advance ratio
ψ	rotor azimuth angle, deg
θ	control angle, deg
Θ	pitch attitude, deg
ϕ	phase angle, deg
Φ	roll attitude, deg
ρ	air density, kg/m^3
Indices	
a	wavelet scaling factor
H	hover
f	frequency domain approach
max	maximum value
ret	retardet
rev	rotor revolution
S	rotor shaft
t	time domain approach
tpp	tip path plane
w	wavelet transform approach

1 Introduction

The reduction of vibration and BVI noise are still 2 of the most important aspects in helicopter research. Hence, the 3 partners ECD, ZFL and DLR are just performing some flight tests, using IBC to reduce the vibration and noise levels in flight. As already introduced in [3], the flight tests concerning the BVI noise investigations subdivide in a first phase, where some open loop tests accompanied by noise measurements on ground were performed, while the second phase that is planned for the end of this year focuses on closed loop control.

For this purpose a suitable feedback signal is required, which is able to provide information about the actual BVI noise condition. Body microphones have proven not always to be suitable, since they are outside the BVI related noise directivity [4]. Taking into account the results and experiences of [1] and [5], it was found that it is best to measure and quantify the effects that occur at the rotor blade itself, which are responsible for the radiated BVI noise. Thus, pressure transducers seem to be the most suitable sensors for the application of a realtime BVI noise identification.

Within the IBC flight tests 3 different algorithms, which are based on the leading edge pressure time histories of the rotating blade, will be examined with regard to their realtime capability and the correlation to the microphone measured noise level at the fuselage of the helicopter as well as on ground. These BVI analysis methods were developed in order to create a feedback signal for closed loop control of BVI noise.

2 The choice of a suitable sensor for BVI noise identification

If one thinks about the identification of the actual BVI noise condition for a helicopter in flight, the first thing is to choose a sensor, which is capable to provide enough information.

2.1 Measurement of the sound pressure with microphones

The direct measurement of noise is normally done with microphones. In the case of rotor noise the resulting signal consists of various portions, corresponding to different sources. The part of noise that has its origin in BVI is restricted to a typical frequency range, so that it can be extracted from the less interesting parts of the microphone measured sound pressure signal. One possibility for this extraction is to compute the so called mid-frequency noise level [1].

$$L_{mid} = 10 \log_{10} \left[\frac{10^{10}}{4} \sum_{i=6}^{40} (a_i^2 + b_i^2) \right] \qquad (1)$$

The coefficients a_i and b_i are the real and imaginary parts of the Fourier coefficients, corresponding to the i^{th} blade passage frequency. Hence, a signal processing, which performs the FFT of the sound pressure signal, is indispensable. As one can see in the frequency spectra of the sound pressure signals measured in the BL and MN trim conditions from [2], Fig. 1, the amplitudes of the spectral lines reach their maximum in the range of the 36^{th} rotor frequency, if there is BVI on the rotor. In addition, the multiples of the blade passage frequency are the dominant parts in the spectrum. For the measurement in Fig. 1 the microphone was arranged at the position $x/R = 0$ and $y/R = 0.82$, see Fig. 2.

Wind tunnel tests [2] have shown that the BVI noise has a strong directivity. For this reason the value of L_{Mid}, determined from a sound pressure signal, depends strongly on the position of the microphone with respect to the rotor. In Fig. 2 the variation of the mid-frequency noise level within a plane below a model rotor is depicted for the BL and MN cases of [2]. The measurement was performed at a vertical distance of $z/R = 1.5$ to the rotor hub. Obviously there are two surfaces in which the BVI noise reaches its maximum for the BL case, one on the advancing and one on the retreating side of the rotor. Taking into account the

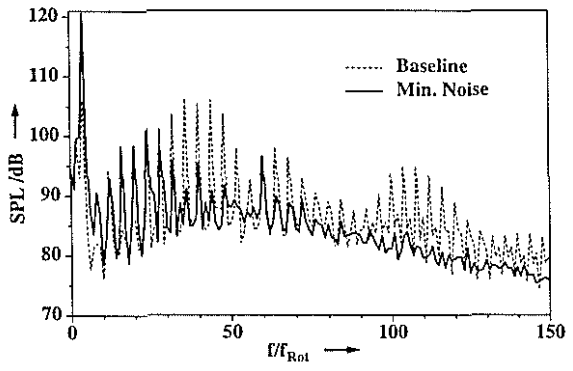

Figure 1: Noise characteristics from FFT of a sound pressure signal for thetrim conditions of the BL and MN cases of [2]

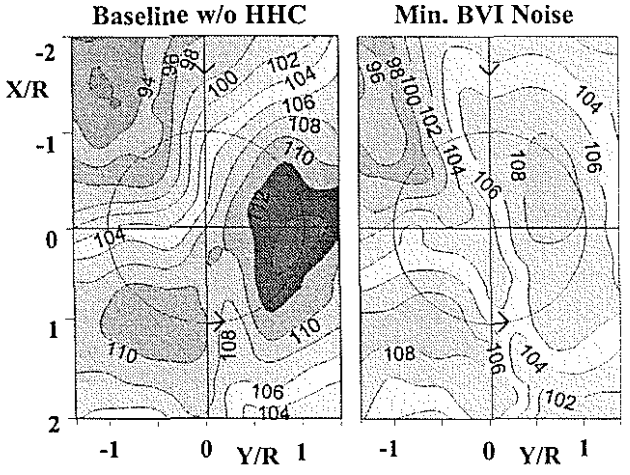

Figure 2: Mid-Frequency (BVI) noise directivities for the BL and MN cases of [2]

directivity of the noise emission, these surfaces are related to the regions on the rotor disk with the most intensive BVI. The positions of maximum BVI noise varies strongly with the trim condition and the HHC input, as can be seen from the comparison of the plots for the BL and MN cases in Fig. 2.

The directivity effect leads to the following conclusion concerning the BVI noise measurement in flight. If the noise is measured directly at the helicopter structure with body microphones, the measurement is at the edge of the noise radiation directivity, in a region that shows a strong noise gradient. Variations in flight condition or rotor control conditions due to IBC inputs may affect the noise measured on the fuselage differently to the noise measured on ground, as the directivity of the noise changes as well. The helicopter fuselage noise often gives an indication of the relative BVI noise changes, corresponding to a certain flight condition, however, the absolute amount of BVI noise heard on ground can not be estimated accurately.

Nevertheless, it is possible to derive the BVI noise intensity, perceived by an observer on the ground, from the near field mid-frequency noise level averaged over a

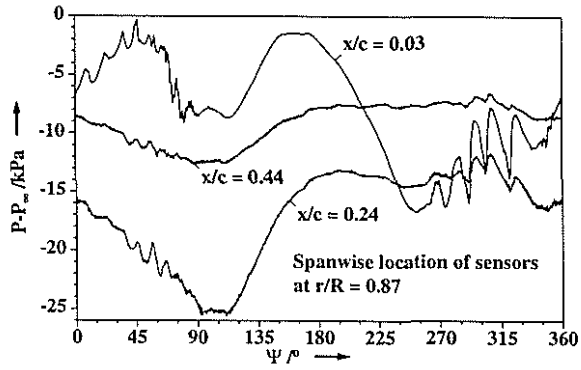

Figure 3: Blade surface pressure histories at different chordwise sensor locations for the BL case of [2]

plane, like in Fig. 2. Getting a representative feedback signal for closed loop BVI noise control from a sound pressure signal measured close to the rotor, one has to mount the corresponding microphone at the position of the maximum BVI noise emissions. As can be seen for the BL case in Fig. 2, these positions lay in the outer parts of the rotor, so that it seems difficult to fix a microphone to the fuselage of a helicopter, which would be able to provide useful data for a BVI noise controller.

2.2 Identification of BVI by blade pressure transducers

A more promising way to get fast information on rotor blade vortex interaction, is to measure the aerodynamic effects that are responsible for the radiated BVI noise directly on the rotor blade. As the interaction of the rotor blade with a vortex affects the pressure distribution on the blade itself, pressure transducers mounted on the rotor blade surface seem to be well suited for the detection of BVI. The chordwise position of the pressure transducer is crucial for the purpose of BVI noise identification by this sensor type. Fig. 3 shows the time history plots of blade pressure signals for one rotor revolution at different chordwise sensor locations for the BL trim condition of [2]. As one can see, every single BVI event is resolvable, using a pressure transducer mounted on the upper side at the leading edge of the blade. BVI events are visible in all of the pressure signals, but they are most clearly to be identified at the leading edge in the vicinity of the airfoils suction peak.

The main characteristic of BVI that can be observed in the pressure histories, is a strong negative gradient, which originates in a sudden rise of the pressure distribution on the upper side of the blade, when it passes the core of the vortex. On the retreating side of the rotor the corresponding gradient of the pressure signal has a positive sign due to the different interaction geometry. Usually in this region the gradients of the pressure time histories are stronger, compared to the

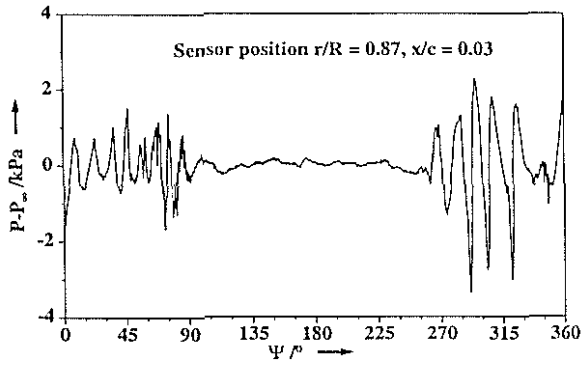

Figure 4: High pass filtered blade surface pressure for the BL case of [2]

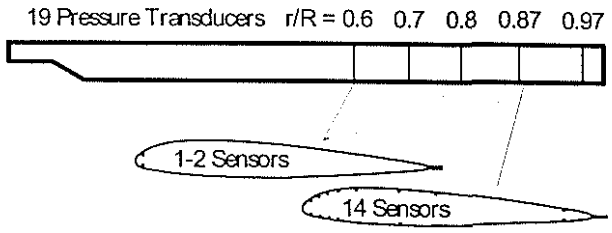

Figure 5: Arrangement of the pressure transducers on the instrumented rotor blade for the IBC flight tests

advancing side, because of a higher value in the circulation of the interacting vortices. This originates from the increased angle of attack at the rotor blade during the vortex creation.

A high pass filtering even allows the detection of weak BVI events. The elimination of the low frequency parts in the pressure histories, which originate from the aerodynamic loading of the rotor, facilitates the identification of the gradients due to BVI. Fig. 4 shows the form of the resulting signal using the input of one of the time histories plotted in Fig. 3. Furthermore, the high pass filtering performs a normalization of the pressure history, so that it can be compared to signals that were recorded under different trim conditions. This is essential for a quantification of the BVI state and the development of a control algorithm for BVI noise, as described later.

The number and the optimum radial positions of the pressure transducers used for these algorithms will be defined later as well, after the sensor instrumentation of the rotor blades, available for the flight tests, has been introduced.

3 Instrumentation & hardware

Since the purpose for closed loop control of BVI noise in flight was the reason for the development of the presented algorithms, the instrumentation and the hardware environment of the used helicopter will be described in this chapter. The testbed for the open loop investigations, performed in march and april of this year, as well as for the planned closed loop tests, is the BO105 S1 of ECD.

The instrumentation in the rotating system consists of 19 pressure transducers on one blade, 3 accelerometers at the rotor hub, 3 accelerometers at the tip of one blade and 2 strain gages on each blade for flapping and lead-lag moment. The arrangement of the pressure transducers on the instrumented rotor blade can be seen in Fig. 5. There are pressure transducers at 5 different radial positions $r/R = 0.6$, 0.7, 0.8, 0.87 and 0.97 at the leading edge on the upper side of the blade that were found out to be well suited for BVI identification. Consequently, these 5 sensors can be used as input for the estimation of the actual BVI state.

The signal processing for the data acquisition begins with an A/D conversion of the signals in the rotating system, which is performed by a transputer based data acquisition system mounted on the rotor hub. The scanning of the signals for the digitalization is triggered to the rotor azimuth angle with 512 samples per rotor revolution. This sampling rate was a compromise of the computing time for the data acquisition and an adequate resolution for the identification of BVI from the pressure histories.

Afterwards, the digitalized data are sent to a second computer in the fuselage of the helicopter, called IBIS, being responsible for the recording of all the data measured in the rotating system as well as for the data of the basis instrumentation. This unit executes also the communication with the ground station via telemetry. For the closed loop tests, the data necessary for noise and vibration control will be provided to the control computer. The real time estimation of the instantaneous BVI state of the rotor is performed by IBIS as well, so that the developed algorithms had to be implemented on this platform.

The demands for the BVI algorithms, concerning the real time capability, are principally determined by the performance of the processing unit, which executes the estimation of the BVI state. The T805 transputer in IBIS that is used for this purpose, is able to perform 2 MFLOPS, which is comparable to a $25MHz$ 386 unit with coprocessor. As only one rotor blade is instrumented with pressure transducers, the used BVI algorithm has to be performed once per rotor revolution. With regard to the rotor frequency of the BO105 helicopter the resulting computation time is $143ms$. This computation is done in parallel to the acquisition of the blade pressure data for the next rotor revolution.

In addition to the pressure transducers on the rotor blade, 3 microphones were mounted at the fuselage of the helicopter for the measurement of the radiated noise due to BVI. The corresponding signals were recorded in analog form, independent of the data acquisition in IBIS. For the synchronisation of the two data sets, the rotor azimuth angle as well as the beginning and the end of an IBIS measurement were also stored

on this analogous tape.

4 Signal processing for the real time estimation of BVI noise

After discussing the suitability of the different sensor types for the BVI identification as well as the most favorable location for the pressure transducers, it is useful to know that the sound pressure time history at any observer position x can be calculated from the blade pressure distribution, using the equation of Ffowcs-Williams/Hawkings [6].

$$4\pi p(x,t) = \frac{1}{c_0}\frac{\partial}{\partial t}\int\int_S \left[\frac{\rho v_n c_0 + l_r}{r(1-M_r)}\right]_{ret} dS + \int\int_S \left[\frac{l_r}{r^2(1-M_r)}\right]_{ret} dS \quad (2)$$

It consists of the thickness noise term, the loading noise term and the quadrupole noise term. The BVI only affects the loading noise term, which can be found as the second term of the sum in the first integral, so that this term will be described in detail.

l_r is the force per unit area pushing on the fluid in the observer direction. In this equation the variable r describes the distance from the source of noise on the rotor blade to the observer position, while M_r represents the Mach number of the source in the observer direction. As one can see, for the exact calculation of the sound pressure signal, using Eq. 2, a large number of pressure transducers is required to get an adequate numerical integration over the rotor blade surface S. Consequently, it is not suited for the real time application of a BVI noise evaluation, because neither the number of the instrumented pressure transducers on the rotor blade, nor the performance of the used computation unit, available for the IBC flight tests, can meet the requirements for solving Eq. 2. Nevertheless, it contains the information about the dominant parameters for the estimation of BVI noise from the blade pressure histories.

4.1 The estimation of BVI noise in the time domain

Looking at the FWH equation, the following issues have to be considered. The gradients of the pressure histories are the dominant indicators for BVI and describe their intensity. A further parameter, important for the intensity of the radiated noise, is the simultaneous rise in the pressure history over a wide radial blade section. The Mach number due to the sensor location is a supplemental factor for the noise relevant weighting of the BVI events. With regard to these facts an algorithm has been developed, working in the time domain, which estimates a quality criterion for the radiated noise due to the BVI events, occuring on the advancing side of the rotor. It consists of 3 parts for the signal processing, depicted in Fig. 6.

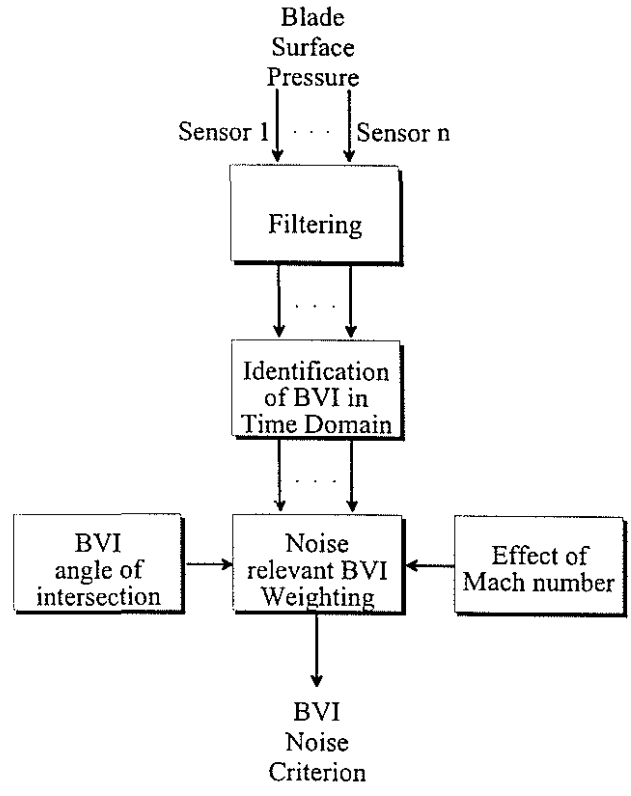

Figure 6: Block diagram of the signal processing for the real time BVI noise identification in the time domain

At first the blade pressure histories of 3 leading edge pressure transducers, mounted at the radial positions $r/R = 0.8, 0.87$ and 0.97, are high pass filtered to eliminate the low frequency parts. The 2 inboard sensor locations at $r/R = 0.6$ and 0.7 were found to be less important for the estimation of the radiated noise. Afterwards, the BVI events can be identified from the resulting signals. Therefore the gradient $\Delta P/\Delta\psi$ is calculated at any sampling location i in the first quadrant for all of the used sensor locations j, using the following equation:

$$\frac{\Delta P_{ij}}{\Delta\psi} = \frac{P_{ij} - P_{i-1,j}}{\Delta\psi} \quad (3)$$

If ΔP_{ij} falls below a specified threshold, baring in mind that it is negative for the advancing side BVI, its value is taken to define the intensity of the corresponding BVI event.

For the resulting share to the quality criterion it has to be weighted due to its significance for the radiated BVI noise. This is done by the introduction of the weighting factors W_M and W_β. The Mach weighting W_M is derived from the FWH equation. Since neither the quality criterion is related to a defined observer position, nor the exact Mach number of the incident flow at the sensor position can be measured in flight, only the share of the blade tip Mach number for the hover-

ing rotor due to the radial sensor location is considered. Thus, the derived weighting factor is only a function of the radial position r_j of the regarded pressure transducer.

$$W_{Mj} = \frac{1}{1 - M_H r_j / R} \tag{4}$$

From Laser Light Sheet measurements in wind tunnel tests [2] it is well known that even BVI events of strong intensity can be less relevant for the noise radiation, if the angle of intersection β_{BVI} between the axis of the vortex and the leading edge of the rotor blade is more than $\beta_{BVI} = 30^o$. For this reason a second factor W_β has been introduced to the algorithm, which considers the angle of intersection for any identified BVI event. W_β is a function of the rotor azimuth angle ψ_i, thus it can be related to the sampling location i, and the radial position of the pressure transducer r_j. The course of curve for $W_{\beta ij}$ is derived from a simple analytical model that determines the angles of intersection β_{BVI} to any position on the rotor disc as a function of the helicopter advance ratio μ.

Simplifying the conditions at the rotor, it is assumed that the vortices are created at the blade tip over the whole region of the azimuth angle in the second and third quadrant of the rotor. Furthermore, it is stated that the increments of the vortices do not change their orientation, if one looks at their projection to the rotor plane, so that the horizontal trajectories looks like Fig. 7. The rotor blades are assumed to have a rectangular shape.

Finally the estimation of the BVI noise from the blade pressure histories can be written in the following form:

$$QC_t = \frac{1}{N_P} \sum_{j=1}^{N_P} \sum_{i=1}^{N_i} \frac{\Delta P_{ij}}{\Delta \psi} W_{Mj} W_{\beta ij} \tag{5}$$

The fraction $1/N_P$ expresses the averaging of the algorithm over the number of pressure transducers, used for the estimation.

4.2 The estimation of BVI noise in the frequency domain

In accordance with the statements of Sect. 2.1, there was the idea to find some characteristics in the frequency spectra of the blade pressure data that can be related to the effects, observed in the frequency spectra of the sound pressure signals, depicted in Fig. 1. Thus, the spectra of the high pass filtered blade pressure data for the BL, the MN and the MV cases of [2], which contain the multiples of the blade passage frequency, are compared in Fig. 8.

But there is no characteristic tendency for the spectral lines in the range of the 36^{th} rotor frequency, which can be observed, comparing the spectra of the different trim conditions. Taking notice of the fact that the used blade pressure data contain the information of the

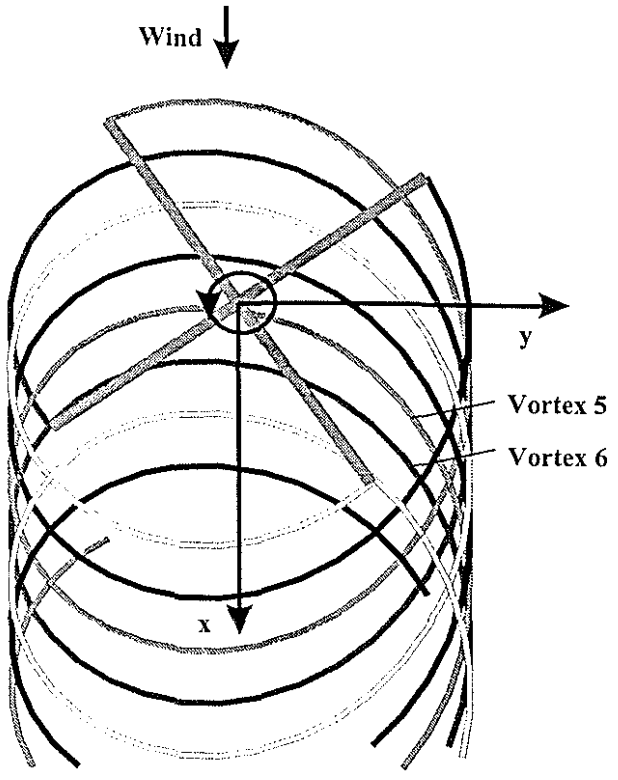

Figure 7: Simplified model of the vortex trajectories projected to the rotor plane

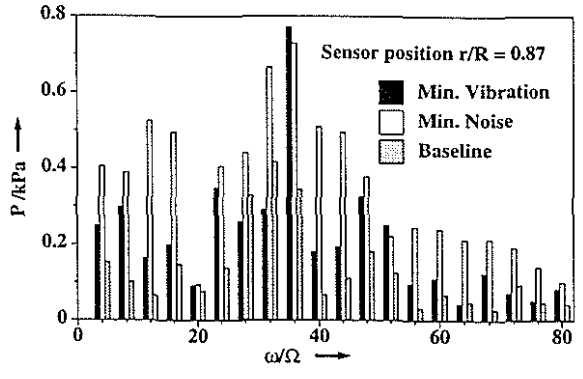

Figure 8: Frequency spectra for the high pass filtered blade pressure data from [2]

parallel interactions as well as the BVI events, less relevant for the noise radiation, a second effort was made. Therefore, the blade pressure data were high pass filtered and subsequently weighted due to the BVI noise relevance, using the function $W_{\beta ij}$, which was introduced in Sect. 4.1. The resulting frequency spectra in Fig. 9 show the rise in the amplitudes of the spectral lines in the vicinity of the 36^{th} rotor frequency for the BL and MV trim conditions, well known from the frequency spectrum of the sound pressure signal for the BL case in Fig. 1. For the MN trim condition the amplitudes of these spectral lines are decreased, while the low frequency part of the 4^{th} rotor frequency is increased, what can be seen in the sound pressure spectrum as well.

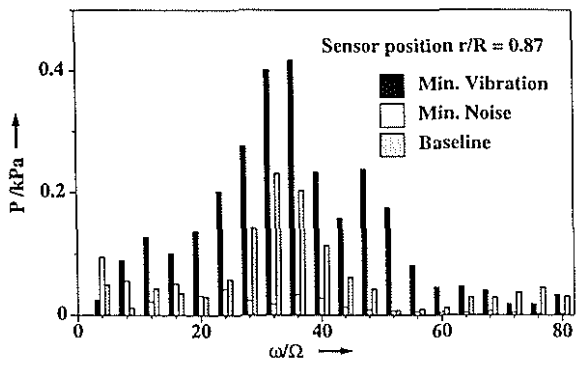

Figure 9: Frequency spectra for the high pass filtered and noise relevant weighted blade pressure data from [2]

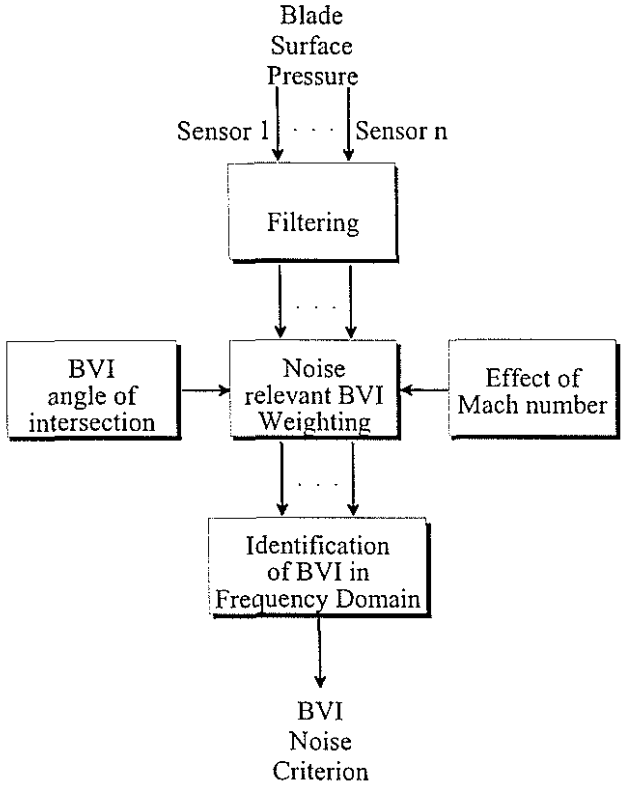

Figure 10: Block diagram of the signal processing for the real time BVI noise identification in the frequency domain

Consequently, an algorithm has been developed, working in the frequency domain and using the representative spectral lines for the estimation of the radiated BVI noise. The block diagram of the corresponding signal processing is shown in Fig. 10.

The algorithm is similar to the one, working in the time domain, except for the fact that the noise relevant weighting is performed previously to the identification of the BVI in the frequency domain. For this algorithm the same 3 leading edge pressure transducers are used as input as for the time domain approach, described in Sect. 4.1. The resulting quality criterion is the sum

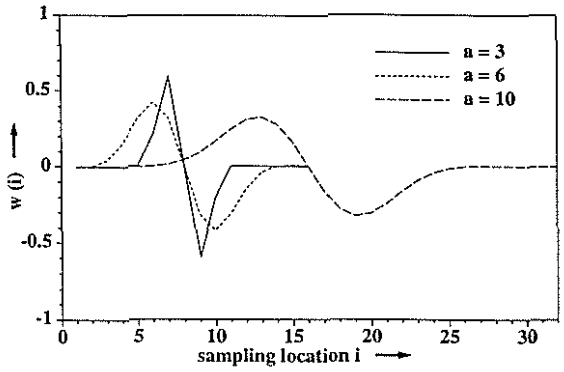

Figure 11: Change of the wavelet form with the variation of the scaling factor a

of the identified amplitudes of the representative rotor harmonics indexed Nk.

$$QC_f = \frac{1}{N_P} \sum_{j=1}^{N_P} \sum_{k=k_1}^{k_2} \sqrt{a_{Nk,j}^2 + b_{Nk,j}^2} \qquad (6)$$

For the BVI identification in the frequency domain, the averaging over the number of the used pressure transducers j is performed as well.

4.3 The estimation of BVI noise by wavelet transforms

A third approach for an algorithm to estimate the radiated BVI noise from blade pressure data was performed by a continuous wavelet transform. This algorithm was developed within a cooperation of Daimler Benz, ECD and DLR. Compared to the algorithm in the time domain, it differs only in the form for the identification of the BVI events. While the time domain approach searches for BVI, looking for a rise in the pressure gradients, the wavelet transform compares the pressure signal with a wavelet that has a typical form of a blade pressure history during BVI. Although the shape of the wavelet is fixed, it can be extended, using different values for a scaling factor a. This purpose allows the adaption of the used wavelet signal to the varying azimuthal extensions of the BVI events in the blade pressure histories. Fig. 11 shows the variation of the wavelet signals with the scaling factor a.

The correlation of the pressure history and the wavelet at any sampling location i in the first quadrant is checked by performing the convolution of the signal and the wavelet.

$$CWT_a(t) = \int_{-\infty}^{\infty} w_a(\tau) P(t-\tau) d\tau \qquad (7)$$

As can be seen in Fig. 12, a negative peak in the resulting signal CWT gives the information about the azimuthal position of a BVI event i_{BVI} in the blade pressure history.

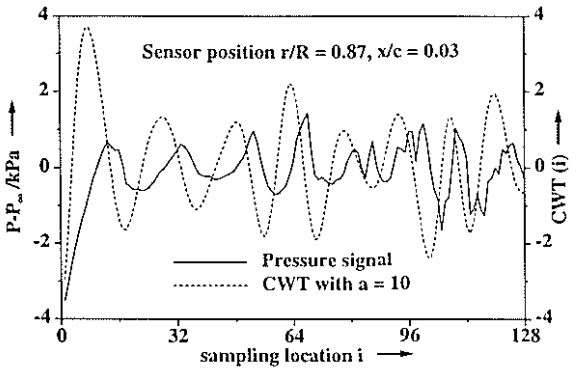

Figure 12: CWT for the high pass filtered pressure history of the BL case of [2], using a scaling factor $a = 10$ for the wavelet

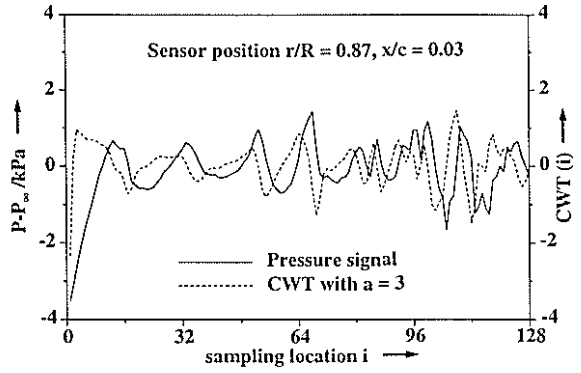

Figure 13: CWT for the high pass filtered pressure history of the BL case of [2], using a scaling factor $a = 3$ for the wavelet

But as the identification of the BVI events depends strongly on the scaling factor a, chosen for the used wavelet, i.e. the interaction in the vicinity of the sampling location $i = 70$ can only be resolved, using a smaller scaling factor of $a = 3$, see Fig. 13.

As the wavelet transform looks for an event, which extends beyond several sampling locations, it is less susceptible to any background noise in the blade pressure signal than the identification described in Sect. 4.1. Compared to the algorithm, working in the frequency domain, it is advantageous that the information of the azimuthal BVI locations is retained. As well as for the estimation in the time domain, the value of the gradient in the pressure history defines the intensity of the BVI event. In opposition to Eq. 5 this algorithm looks for the maximum value of ΔP_i at the adjacent sampling locations $\Delta i = \pm 3$ of the identified BVI location i_{BVI}. Consequently, for any BVI event only one value of the corresponding pressure gradient is added to the quality criterion. The following signal processing, performing the noise relevant weighting, is equal to the one, used in Sect. 4.1.

But as the BVI locations are predictable with an accuracy that corresponds to the sampling rate, it is imaginable to determine the BVI location with the minimum in the angle of intersection $\psi(\beta_{min})$, using the information of at least two blade pressure transducers. This azimuthal position of the most parallel BVI, occuring in the first quadrant of the rotor, could be used for an azimuthal shifting of the weighting curve $W_{\beta ij}$. In this way, the analytical model for the BVI angles of intersection β_{BVI} can be adapted to the changes in the wake geometry, according to the flight condition of the helicopter. The described signal processing for the estimation of BVI noise by wavelet transforms can be seen in Fig. 14.

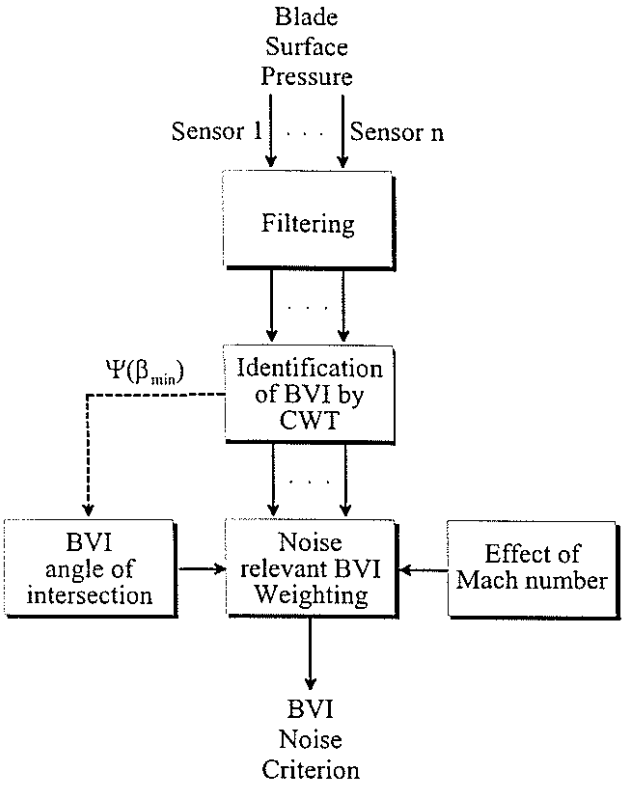

Figure 14: Block diagram of the signal processing for the real time BVI noise identification by CWT

5 Validation of the BVI analysis using wind tunnel data

For the development and adaption of the 3 presented BVI analysis methods by blade pressure signals, especially the data of the measurements in [2] were used. There are a few reasons for this decision. First, in these wind tunnel tests extensive measurements of the radiated noise due to BVI below the rotor were performed that could be used for a correlation test of the BVI analysis output to the measured noise level. Second, the blade pressure data with a high resolution of 2048 samples per revolution were available and well suited as input for the analysis methods. Third, the measurement implied the effect of HHC inputs on the BVI noise emissions, what is useful with regard to the planned

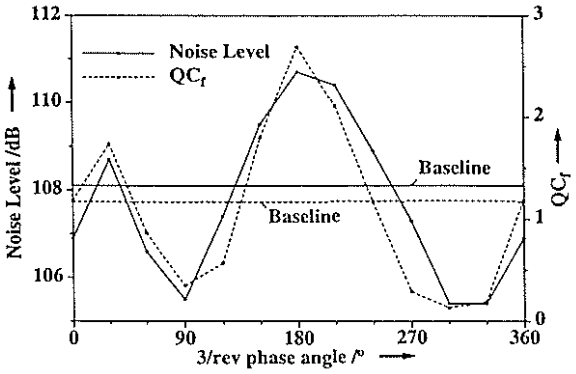

Figure 15: Noise Level and output of BVI analysis in the frequency domain for the $3/rev$ phase variation of [2]

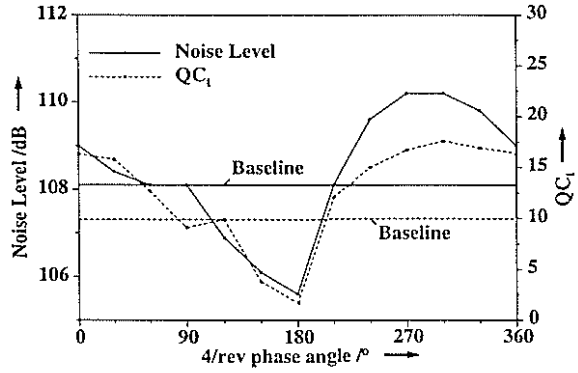

Figure 16: Noise Level and output of BVI analysis in the time domain for the $4/rev$ phase variation of [2]

IBC flight tests.

For the correlation test with respect to the phase variation, corresponding to $3/rev$ and $4/rev$ HHC inputs with amplitudes of $\theta_3 = 0.85^o$ and $\theta_4 = 0.85^o$, the averaged time histories of the blade pressure data were employed. Fig. 15 shows the results of the BVI noise estimation in the frequency domain for the $3/rev$ phase variation from [2]. Besides the HHC phase angle of $\phi_3 = 270^o$, a good correlation of the BVI analysis output with the measured noise level was achieved. The most important feature for an adequate curve fitting was the adaption of the weighting function W_β due to the BVI angles of intersection. As the quality of the correlation is similar for the approaches in the time domain and by wavelet transforms, these curves are not depicted explicitely.

For the IBC flight tests it was planned to investigate the effect of a $2/rev$ IBC input on BVI noise. As for the HART tests no measurements for this input could be performed, the analysis outputs were tested to proof the correlation to the noise measurements for the $4/rev$ phase variation, just to show that the application of the algorithms is not limited to the estimation of BVI noise at higher harmonic inputs of $3/rev$. The curve of the analysis in the time domain in Fig. 16 gives good correlation with the microphone measured noise level as well. Especially the HHC phase angle for the minimum noise condition can be well fitted by the analysis output.

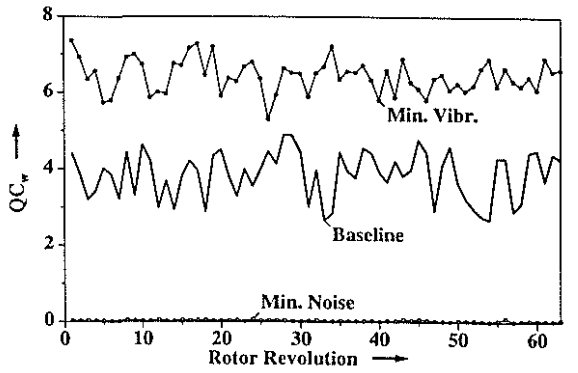

Figure 17: Single time histories for the output of the BVI analysis by wavelet transforms for the BL, MV and MN trim conditions of [2]

Finally Fig. 17 shows the quality criterion, estimated by wavelet transforms, using different single time histories of the blade pressure data, as the instantaneous variation of the analysis output is most important for the closed loop tests that are planned for the end of 1998. The curves for the BL and MV cases with intensive BVI exhibit large variations, although the trim condition of the rotor is thought to be steady in the wind tunnel. Nevertheless, the differences of the mean values for the chosen trim conditions are confirming the corresponding noise levels in Fig. 15.

6 Results from the flight tests

After the different approaches for the BVI analysis were validated in Sect. 5, using wind tunnel data, finally the results from the IBC flight tests shall be discussed. At first, the analysis of the flight conditions for the time intervals of the data recording in the helicopter will be described. Furthermore, the correlation for the single time histories of the BVI analysis outputs with the noise measurements of the microphones, mounted at the helicopter fuselage, will be shown. The mean values of the different quality criteria QC_t, QC_f and QC_w for the phase variations with $2/rev$ IBC input will be compared to the noise measurements on ground. In addition, the results of rotor simulations with IBC input will be presented in order to encourage the understanding of the observed phenomena.

6.1 The analysis of the flight condition

The angle of attack of the tip path plane α_{tpp} is the most important parameter for the origin of BVI noise on a helicopter rotor, which is a well known fact from wind tunnel tests. In [2] it is stated that even for flight tests α_{tpp} is a function of the rotor thrust coefficient

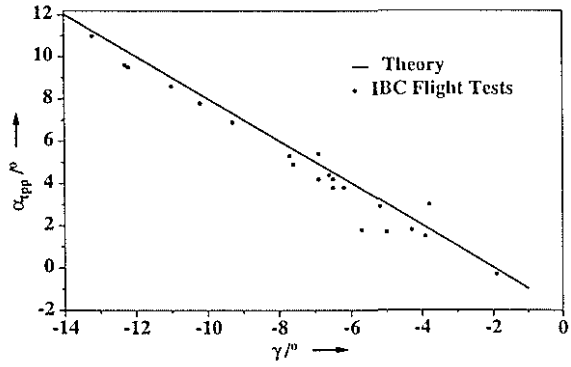

Figure 18: α_{tpp} versus γ from theory [2] and the flight path angle variation of the IBC flight tests

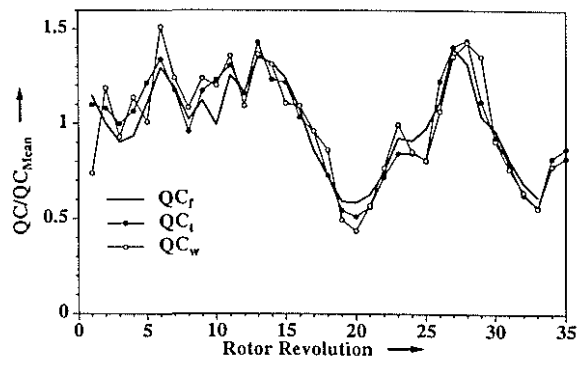

Figure 19: Single time history output of the different BVI analysis methods for the BL case of the IBC flight tests

C_T, the advance ratio μ and the flight path angle γ.

$$\alpha_{tpp} = -\gamma - 0.44\frac{\mu^2}{C_T} \tag{8}$$

Hence, for constant values of μ and C_T the tip path plane angle of attack should be a linear function of the flight path angle γ. For a helicopter in a steady descent flight condition the rotor thrust coefficient C_T can be related to the helicopter weight m, while μ is proportional to the helicopter speed V. Consequently the tip path plane angle of attack α_{tpp} for a helicopter rotor in steady flight, must be a linear function of γ as well, if m and C_T are constant during the time interval of the measurement.

For the analysis of the IBC flight test data with regard to the important parameter α_{tpp}, it is assumed that it can be derived from the following equation.

$$\alpha_{tpp} = -\gamma + \Theta - \epsilon - \beta_{1C} \tag{9}$$

The variable Θ is the pitch angle of the helicopter, while $\epsilon = 3^o$ is the constant tilt angle of the rotor shaft to the vertical axis of the fuselage. β_{1C} describes the distortion of the tip path plane to the rotor shaft in pitch direction and is derived from the cosine part of the first rotor harmonic in the mast bending moment.

Comparing Eq. 8 and Eq. 9 it must be assumed that the last 3 terms in Eq. 9 are constant for a descent flight with fixed speed and of course constant weight of the helicopter during the time interval of one landing approach. In Fig. 18 the results of the IBC flight tests from the variation of the flight path angle γ are compared to the theoretical curve of [2]. As there is a good correlation of the flight test data with the theory, for most of the data points it should be sufficient to look at the value of the flight path angle γ to get a first approximation of the rotor trim condition with regard to the BVI noise emissions. If the trim condition shall be examined in detail, the additional parameters of Eq. 9 have to be considered.

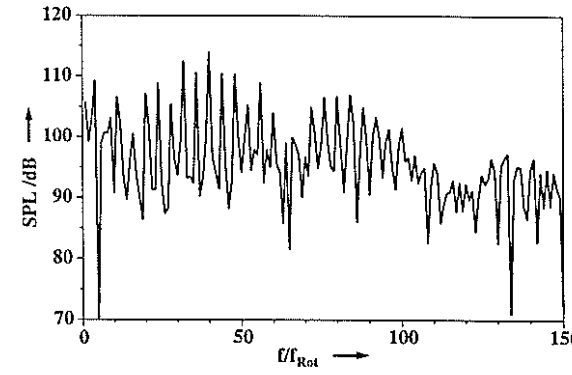

Figure 20: Fourier spectrum of the sound pressure level at the body microphone 2 for the Bl case of the IBC flight tests

6.2 Correlation of the BVI analysis outputs with noise measurements

As already shown for the wind tunnel data in Fig. 17, the single time history output of the BVI analysis varies strongly over the duration of several rotor revolutions. A similar behaviour can be observed looking at the single time histories for the quality criteria, corresponding to a BL case of the IBC flight tests. As the analysis outputs in Fig. 19 show large variations over the duration of the measurement, the data recorded at the 3 body microphones are used to check the relative shape of the curves.

In Fig. 20 one can see that the Fourier spectrum of the data recorded at one of these microphones show the rise in the parts close to the 36^{th} rotor frequency, which is typical for the occurence of BVI and could already be seen in Fig. 1.

The comparison of the quality criteria with the time history plots of the mid-frequency noise levels from the body microphones gives a good correlation, see Fig. 21 and Fig. 19. For this reason all of the 3 BVI analysis algorithms seem to be well suited to identify the instantaneous changes in the BVI noise emissions of the rotor.

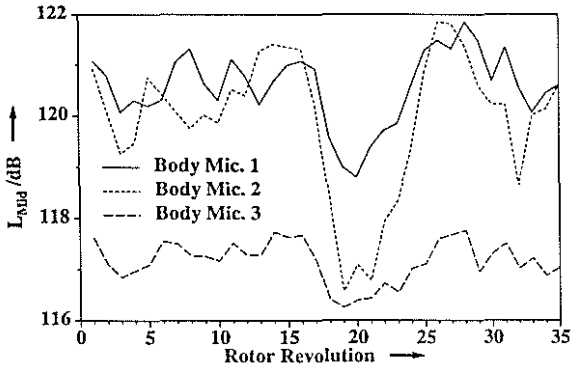

Figure 21: Single time history of L_{mid} from the body microphones for the BL case of the IBC flight tests

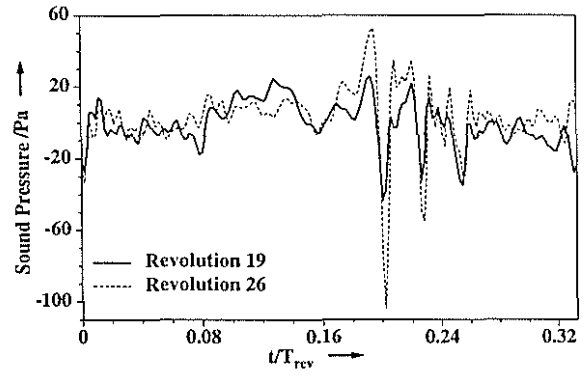

Figure 22: Sound pressure time history from the body microphone 2 for the minimum and maximum value of L_{mid} inFig. 21

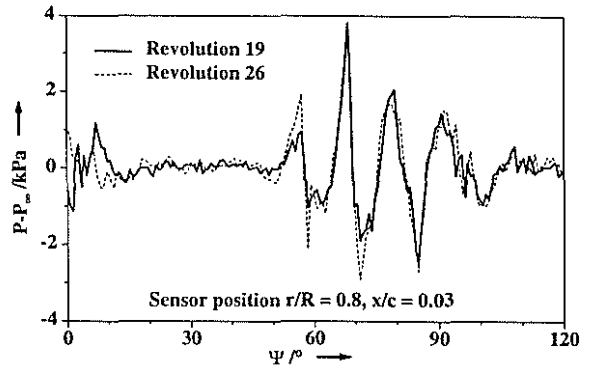

Figure 23: Blade pressure time history for the minimum and maximum value of QC inFig. 19

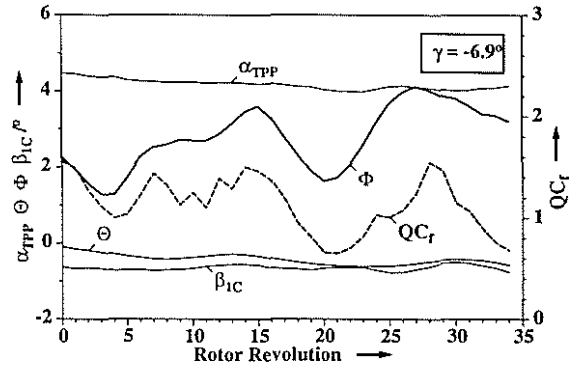

Figure 24: Analysis of the flight condition for the BL case of the IBC flight tests

This can be emphasized by looking at the sound and pressure histories, depicted in Fig. 22 and Fig. 23. The difference in the amplitudes of the sound pressure signal from revolution 19 and 26, corresponding to the minimum and maximum values of the noise level from the body microphone 2 in Fig. 21, as well as for the analysis outputs in Fig. 19, can be related directly to the intensity of the BVI in the blade pressure signals. As the distances from the BVI locations on the rotor blades to the microphones at the fuselage of the helicopter are small, the transit-time effect is negligable.

But there is still the question, where the differences in the BVI intensities derive. The analysis of the flight condition for the considered BL case in Fig. 24 shows small variations for the pitch angle Θ as well as for β_{1C} over the time duration of the measurement. But the BVI analysis output QC_f seems to give a good correlation with the helicopter bank angle Φ. This correlation can be observed principally in the time history plots of the BL cases at flight path angles of $-6^o > \gamma > -9^o$, where the blade vortex misdistances in the critical regions of the rotor are small, and consequently, the BVI noise emissions are high. In this case a dynamic excitation of the helicopter in the roll axis seems to affect the blade vortex misdistances during BVI, what can be responsible for the instantaneous changes in the radiated noise.

The time history plot of QC_f for a trim condition with a smaller flight path angle of $\gamma = -5.2^o$ shows that a comparable excitation in the roll axis of the helicopter, like in the BL case in Fig. 24, does not affect the quality criterion QC_f in a comparable manner, see Fig. 25. One possible interpretation of this phenomenon could be that the blade vortex misdistances in the critical ranges of the first quadrant of the rotor are increased due to the decreased value of α_{tpp}, what is confirmed by the decreased mean value of QC_f for this measurement. Thus, even a strong excitation in the rolling motion shows no visible effect on the noise emissions.

After the BVI analysis methods were proven to indicate the instantaneous changes in the noise emissions of the rotor in flight, their suitability for the identification of the changes in the BVI noise due to the IBC inputs on the rotor will be examined. Therefore, the mean values of the analysis outputs will be compared to the results of the noise measurements on ground for the phase variation of the $2/rev$ IBC input with an amplitude of $\theta_2 = 1.0^o$. In Fig. 26 the variation of the maximum noise level on ground with the $2/rev$ phase angle is compared to the BL case. It is important to know that the noise measurements on ground exhib-

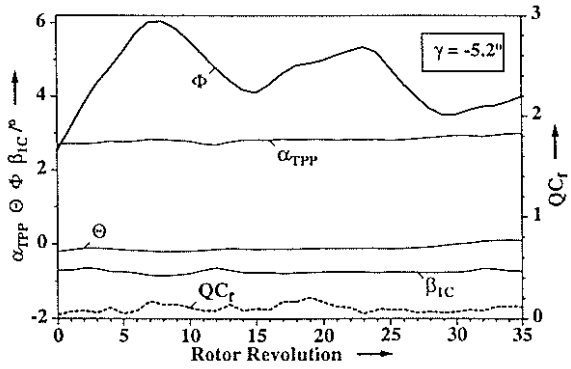

Figure 25: Analysis of the flight condition for a descent flight of the IBC flight tests with $\gamma = -5.2^o$

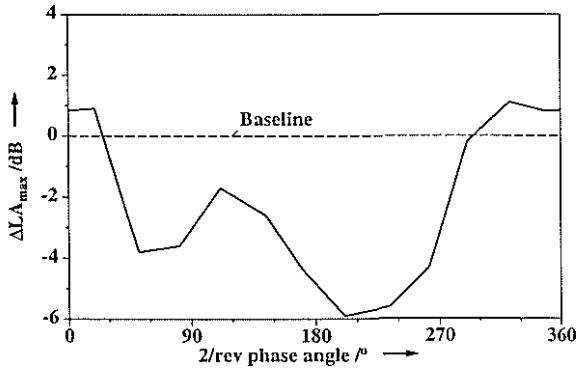

Figure 26: Variation of the uncorrected maximum noise level on ground with the $2/rev$ phase angle from the averaging over 11 microphones [7]

ited large variations for the noise levels at constant IBC trim conditions of the rotor, which are described in [7].

There are 2 local minima in the ranges of $\phi_2 = 60^o$ and $\phi_2 = 210^o$. In addition, the BVI noise can be reduced over a large range of the $2/rev$ phase angle.

The variations of the BVI analysis outputs with the $2/rev$ phase angle are depicted in Fig. 27. As the outputs of the different analysis methods have different ranges, all the values are related to the value of the BL case.

The local minima can be found at the same phase angles as for the noise measurements on ground in Fig. 26, but there are differences in the absolute values. Especially, the increased value of the quality criteria at $\phi_2 = 120^o$, which is higher than the value for the BL case, can not be confirmed by the noise measurements in Fig. 26. In addition, the minimum of the quality criteria extends over a larger range of the $2/rev$ phase angle than the curve of ΔLA_{max}.

As one reason, it can be supposed that the different durations of the data recording for the measurements on ground and in the helicopter can be responsible for the differences in the curves of Fig. 26 and Fig. 27. Whereas the measurement in the helicopter bases on a recording time of $5 - 6s$, the duration of the noise measurements on ground for one approach of the heli-

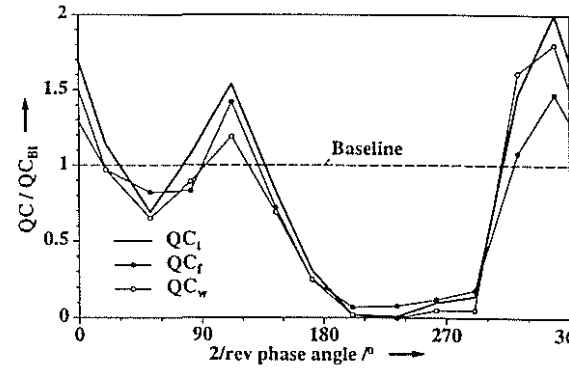

Figure 27: Variation of the quality criteria with the $2/rev$ phase angle from the blade pressure analysis in the helicopter

copter lasts about $25s$. During this time interval, the trim condition of the helicopter could have changed substantially, so that for the moment of the noise radiation, corresponding to the value of LA_{max} on ground, the data recording in the helicopter could be inactive. I.e. the extension of the second minimum to the $2/rev$ phase angle of $\phi_2 = 300^o$, which can be observed in the curves of Fig. 27, is assumed not to match the reality. The reason for the small values of the quality criteria can be found in the flight path angle γ. It was analysed to be $\gamma > -5^o$ for all of the 3 data points, corresponding to $\phi_2 = 300^o$, during the time interval of the data recording in the helicopter. The nominal value for the measurements was $\gamma = -6^o$, so that the flight condition for these measurements are not acceptable.

6.3 DLR Rotor Code S4

The DLR rotor code S4 originally was developed to compute effects of HHC onto dynamic rotor forces of a hingeless rotor in the nonrotating frame [8, 9]. With time, it evolved into a comprehensive rotor code with lots of features in an aerodynamics, structural dynamics and control sense. It is nowadays mainly used to compute high resolution blade loads for acoustic post-processing of rotors under active control of HHC or IBC [10], but also for investigations of dynamic stall [11] and for parametric rotor optimization. It mainly consists of 3 modules: the aerodynamics, the structural dynamics and the induced velocities module. They are embedded in a trim algorithm and comprise:

a) The aerodynamic module (Literature in [12, 13, 14]), either:

- linear aerodynamics [no aerodynamics / steady model / unsteady model (incl. varying velocity effects)] or:
- nonlinear aerodynamics (incl. Mach effects) [steady model (incl. steady stall) / unsteady model (incl. dynamic stall and varying velocity effects) / both with or without yaw influence]

b) The structural dynamics module is able to deal with articulated or hingeless rotors of arbitrary blade numbers. In both cases, the rotor blades are described by

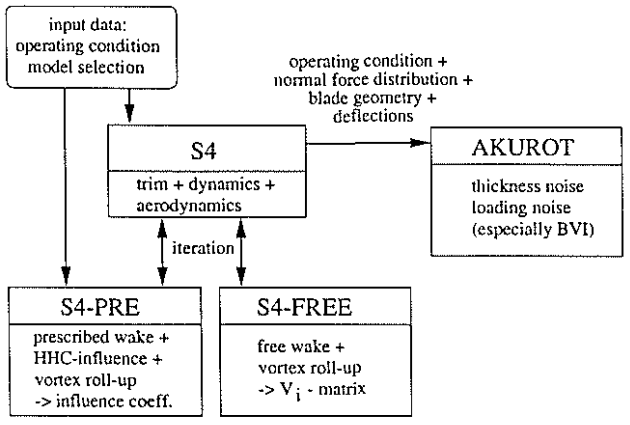

Figure 28: Computational scheme for rotor simulation/acoustic emission

their mode shapes in flap, lead-lag and torsion separately. Their dynamic behaviour is represented by their rotating natural frequencies as a function of the rotating speed. Both the mode shapes and the natural frequencies are taken from either experiments or usually from finite element computation. Within the rotor code the generalized coordinates of each mode are computed by time integration of their differential equations of motion, having the generalized aerodynamic forcing on the right hand side of the equations. For this purpose, a Runge-Kutta 4^{th} order scheme is used. This module features the following options: [no modes (=rigid blades, propeller case) / flap, lag, torsion modes (individually or together) / prescribed or free motion of the modes]

c) The third important module is associated with the induced velocities. These are either: [constant (either prescribed or thrust related) / trapezoidal / nonuniform (Mangler/Squire, [15]) / prescribed tip vortex wake (Beddoes geometry, [16]) / free-wake [18] / rotor-body interactions and wind tunnel-body interactions [17]].

The overall handling is done with a trim module [no trim / manual trim / automatic trim] for specified non-rotating hub forces/moments. As degrees of freedom to trim to the desired values, the collective and cyclic controls are used; optionally the rotor shaft angle of attack can be taken as additional means of control. There also is an interface for any HHC controller. Acoustic postprocessing is done at the DLR institute for design aerodynamics, where the load distribution of the S4 program is used as input for the FWH equation. The program scheme is sketched in Fig. 28.

For simulation of the IBC cases the following combination is used: nonlinear unsteady aerodynamics including yaw; hingeless blades with 3 flap modes, 2 lead-lag modes and 1 mode in torsion; prescribed wake geometry including HHC effects; trim to thrust, pitch and roll moment at given airspeed and shaft angle of attack (the latter values taken from the flight tests).

6.4 Computation of IBC effects

For analysis of the IBC effects on the BO105 main rotor noise emission the S4 code is used in the following form. First, from the experiments a typical rotor condition is chosen. This provides data for the rotor operating condition like C_T, μ, α_S and rotor roll and pitch moments M_x and M_y. Then, the S4 code is run for the BL case first, trimming for the desired values of thrust and moments under constant global conditions (μ, α_S). Iteratively, the wake geometry and blade dynamics simulation is done. Typically, 2 iterations are enough to obtain convergence. Afterwards, the IBC variations are done in the same way: prescribing the IBC control to $\theta_2 = 1^o$ and $\phi_2 = 0^o$, 30^o, ..., 330^o and trimming again to thrust and moments of the BL condition, as the pilot did when flying the helicopter.

Since the S4 code essentially is based on lifting line theory, no pressure distribution is available from the code. On the other hand, due to scarse instrumentation of the BO105 rotor blade, no local loading nor blade deflections are available for direct comparison. However, the blade leading edge pressure distribution can be obtained from the transducers at $x/c = 0.03$ on the upper surface. They are very sensitive to changes of oncoming flow conditions and thus are a useful indicator of where BVI occurs, where the vortices are flying on top of or below the rotor disk, and where they penetrate the disk. When applying a high pass filter suppressing the lowest $6/rev$ frequencies that contain mainly dynamic pressure and blade motion components, the remaining pressure distribution is originating principally from BVI events, i.e. the upwash and downwash of individual vortices coming close to the blade leading edge. This can be compared to the induced velocity distribution of the simulation, filtered in the same way.

In Fig. 29 the BL case pressure distribution of an individual revolution of the flight test at nominal 6^o descent is compared to the BVI locations in the simulation, also trimmed for 6^o descent flight. The simulation obviously predicts the vortices to penetrate the rotor disk at the most critical locations for BVI noise emission, i.e. where the vortices are parallel to the rotor blade leading edge. The flight test, however, does not show this in that detail. Here, the vortices do pass the disk earlier, i.e. at azimuths of about $\psi = 70^o$ on the advancing and at $\psi = 280^o$ on the retreating side.

Changing the flight path to only $\gamma = 4^o$ descent in the simulation gives the BVI locations of Fig. 30, which compare much better to the flight test, especially on the advancing side. A reason for this behaviour may be found in the wind conditions during the test: probably the effective flight path was not the same as the geometrical flight path due to head wind. Another possibility of this discrepancy may be in the assumptions of the basic wake geometry with rotor moments near zero, a trim condition that has been used for the wind tunnel tests of [2]. In the flight test, a strong pitch moment in the range of $2000Nm$ was measured, and the

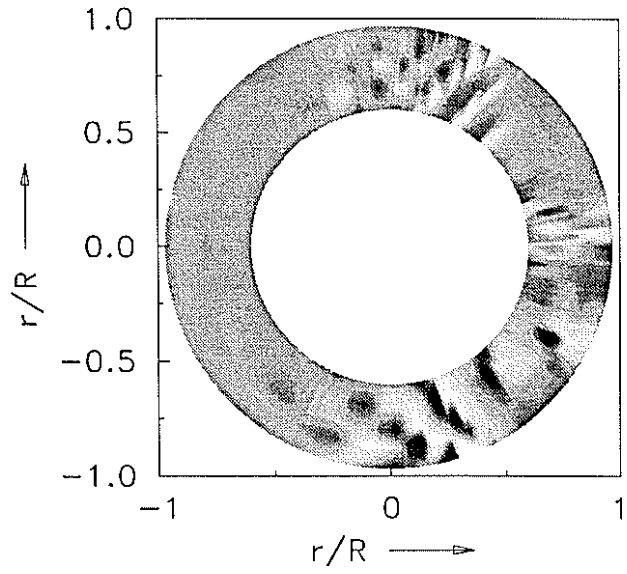

(a) Flight test: leading edge pressure distribution, h.p. filtered at $6/rev$.

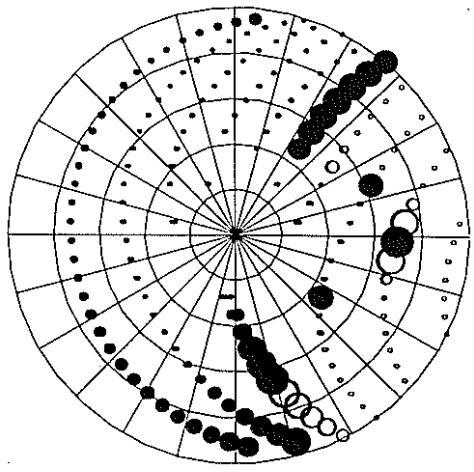

(b) Simulation: BVI locations. Vortices are above the disk (solid symbols) or below (open). Symbol thickness indicates closeness to the blades

Figure 29: Comparison of BVI locations in the rotor disk for the BL case (6^o descent, $C_T = 0.0059$, $\mu = 0.15$)

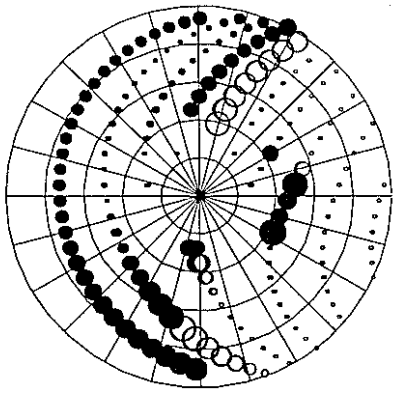

Figure 30: BVI locations from simulation at 4^o descent, $C_T = 0.0059$, $\mu = 0.15$

lift for that moment must have been created about 80^o earlier in azimuth. Following the assumptions of momentum theory, this will cause extra downwash on the advancing side and some upwash on the retreating side relative to the condition with zero moments. Tip vortices thus will be convected more downwards on the advancing side and the penetration of the rotor disk will shift to higher azimuth positions.

The implementation of steady aerodynamic moments into the prescribed wake geometry will be done in the near future. However, as a reference for the simulations the 6^o descent was chosen and the changes of the wake structure relative to the BL case due to IBC are the important features to represent.

The quality criterion in the time domain used for analysis of the blade leading edge pressure as an indicator for the noise emission of the rotor can also be applied to the unsteady simulated rotor blade loading, either based on the local forces $dL/dr(r,\psi)$ or their nondimensional equivalent $C_n M^2(r,\psi)$. This is done for the phase sweep of the $2/rev$ IBC and depicted in Fig. 31(a). Here, as in the quality criterion applied to the pressure time histories, only the advancing side is taken into account. It can be seen that in most of the IBC control settings a reduction of the quality criterion is achieved, with a minimum at $\phi_2 = 180^o$ and a second minimum at $\phi_2 = 30^o$, while a slight increase is indicated at $\phi_2 = 90^o$ and between $270^o \leq \phi_2 \leq 330^o$. Compared to the quality criterion from the blade pressures, this curve appears to have a shift of about $\Delta\phi_2 = 30^o$, but the essential features are very similar. In terms of rotor azimuth, this shift reduces to half the value and is within the uncertainty of the HHC wake deflection algorithm used for the prescribed wake. Nevertheless, the important features are represented.

Also shown is an intrusion index I_I, based on the $4/rev$ component of the vertical hub force in the simulation results, which is compared to the appropriate hub acceleration from the flight tests (Fig. 31(b)). Again, a difference in the IBC phase is observed between experiment and simulation, but the general behaviour is represented. In contrast to the HART test with $3/rev$ HHC, where vibrations are large when the noise is low and vice versa, here, an IBC phase area is present, where noise and vibrations simultaneously are reduced in the range of $330^o \leq \phi_2 \leq 45^o$).

At the minimum of the quality criterion for BVI noise, the measured pressure distribution will be com-

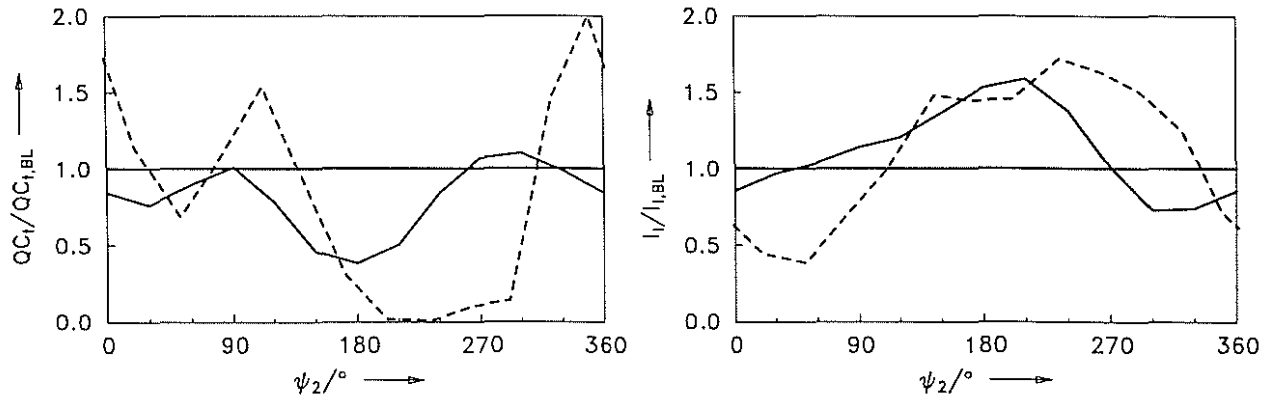

(a) QC_t based on loading from simulation (solid) and based on pressure histories from flight tests (dashed)

(b) I_I based on $4/rev$ vertical hub force from simulation (solid) and hub accelerations from flight tests (dashed)

Figure 31: Variation of the quality criteria for BVI noise and vertical vibrations with IBC phase. $\theta_2 = 1°$, condition as in Fig. 29

pared again to the BVI locations from simulation. This is given in Fig. 32. Compared to Fig. 29, the tip vortices appear to penetrate the rotor disk earlier, at azimuth angles of $\psi = 90°$ on the advancing side and at $\psi = 270°$ on the retreating side. The entire area downstream is free from BVI, because the vortices are far below the disk there and this is the reason, why the noise emission is reduced so much. The same behaviour was found at $3/rev$ HHC control in the wind tunnel [5]. In the simulation result, also compared to the BL case of Fig. 29, it is clearly visible that the important parallel BVI occuring at $\psi = 50°$ has no effect anymore, since this vortex now is far below the rotor. The essential behaviour of the vortex flight path, namely to penetrate the rotor disk at $\psi = 90°$, where the blade vortex interaction angle β_{BVI} is large, is computed well.

Next the local loading of the simulation will be analysed. For noise emission, the time derivative of the local loading is important, and this is the basis for the quality criterion. In Fig. 33 the time derivative of the loading $\Delta C_n M^2$ in the first quadrant of the BL case is given before and after multiplication with the weighting functions W_M and W_β. It can be seen that important blade parallel BVI exists, and the weighting function reduces all non-parallel BVI to a lower level. The positive weighted gradients are summed up to form the quality criterion.

When the quality criterion is minimum, then these loading gradients at blade parallel BVI are reduced, while they are increased at locations that are not important for noise emission. This can be seen in Fig. 34, where the same procedure is applied to the loading of the $2/rev$ IBC case with $\theta_2 = 1°$ and $\phi_2 = 180°$. Compared to Fig. 33, the loading gradients at the blade parallel BVI (around $45°$) are reduced significantly, while they are increased at larger values of ψ.

The reason for this behaviour of the vortex flight path can be analysed by the basic rotor loading distribution, given in Fig. 35 for the BL and MN quality criterion case. Here, only the frequency content up to the 6^{th} harmonic is included in order to separate the BVI induced loading from the basic rotor loading. The $2/rev$ IBC control produces additional lift around $\psi = 90°$ and $\psi = 270°$, thus increasing the local downwash there. The tip vortices, created at the front of the disk, have to pass these additional downwash areas and therefore are pushed down to a lower flight path within the rotor disk, compared to the BL case. The same functionality has been observed in the wind tunnel tests of the HART program at $3/rev$ HHC, see [10, 5].

7 Conclusions

In this paper, the development and validation of analysis methods for a realtime BVI noise identification from blade pressure data are described. The conclusions can be summarized as:

- Pressure transducers were found to be suitable sensors for a realtime BVI analysis in flight, being located at the leading edge on the upper side of the rotor blade.
- On the basis of these sensors, 3 different BVI analysis methods were developed, which handle the data in the time domain, the frequency domain or by continuous wavelet transforms.
- The analysis methods could be validated, using the data for the phase variation of the $3/rev$ and $4/rev$ HHC input from wind tunnel tests.
- The single time histories of the analysis outputs can be correlated with the noise, measured at the body microphones of the helicopter in the IBC flight tests. Hence, the algorithms are proved

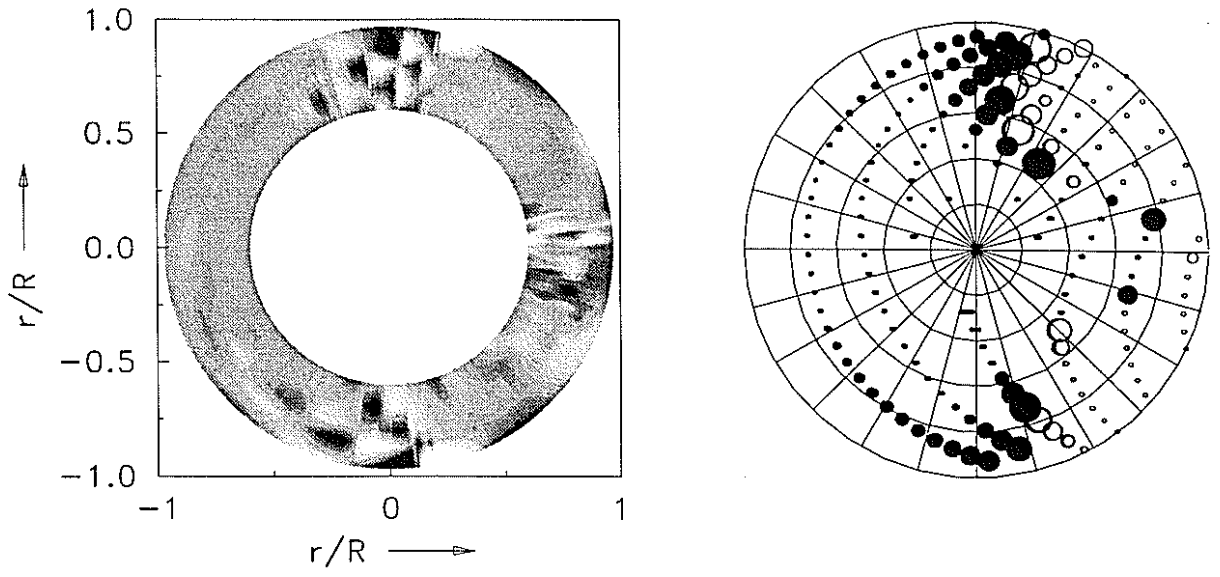

(a) Flight test: leading edge pressure distribution, h.p. filtered at $6/rev$.

(b) Simulation: BVI locations. Vortices are above the disk (solid symbols) or below (open). Symbol thickness indicates closeness to the blades

Figure 32: Comparison of BVI locations in the rotor disk at the minimum of QC_t in Fig. 31, condition as in Fig. 29

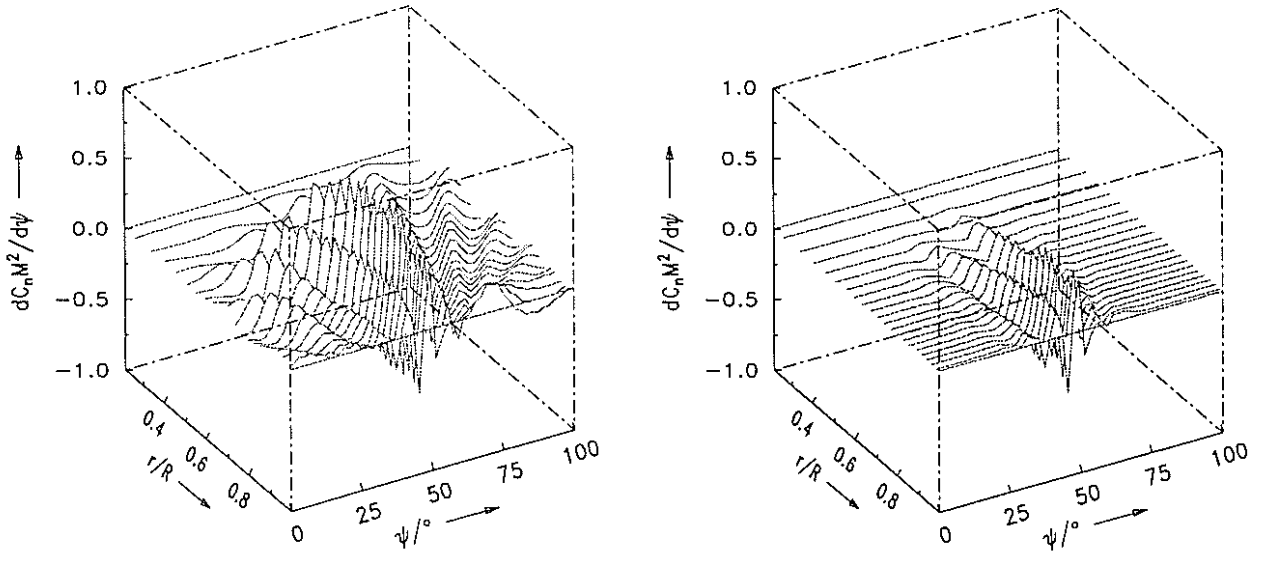

(a) original data

(b) multiplied with $W_M W_\beta$.

Figure 33: Time derivative of the simulated loading distribution ($dC_n M^2/d\psi$) for the BL case, h.p. filtered at $6/rev$, condition as in Fig. 29.

to identify the instantaneous changes in the BVI noise emissions of the rotor.

- The changes in the single time histories of the noise emissions were found to originate from variations in the trim condition of the helicopter. Especially for the BL cases with strong BVI noise emissions a correlation of the analysis outputs, as well as of the noise measured at the body microphones, with the rolling motion of the helicopter can be observed.

- The mean values of the analysis outputs for the phase variation of the $2/rev$ IBC input with an amplitude of $\theta_2 = 1.0^o$ gives good correlation with the noise measurements on ground. Above all, the local minima in the measured noise levels on ground at the phase angles for $\phi_2 = 60^o$ and $\phi_2 = 210^o - 240^o$ can be found in the curves of the

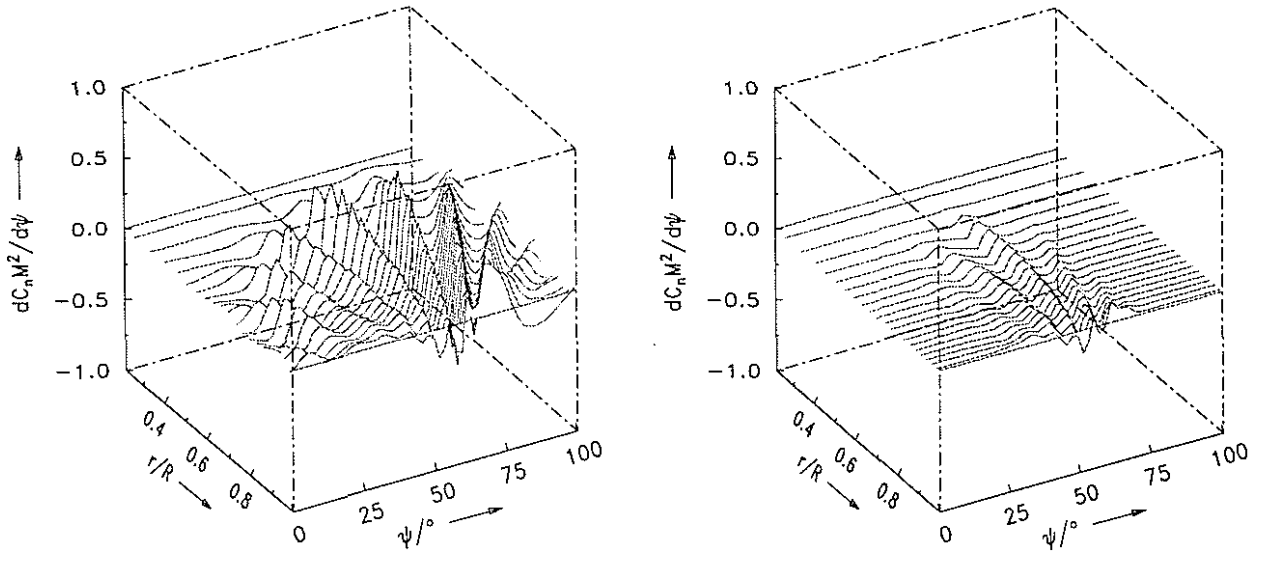

(a) original data

(b) multiplied with $W_M W_\beta$.

Figure 34: Time derivative of the simulated loading distribution ($dC_nM^2/d\psi$) for the minimum of QC_t in Fig. 31, h.p. filtered at $6/rev$, condition as in Fig. 29

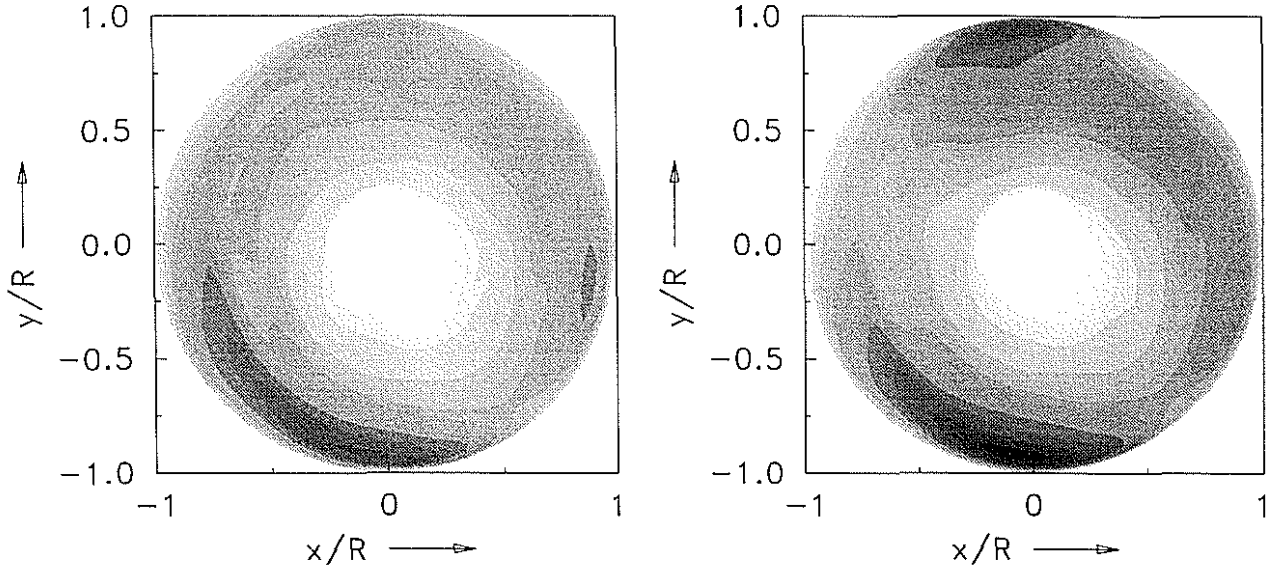

(a) BL case

(b) IBC with $\theta_2 = 1°$ and $\phi_2 = 180°$

Figure 35: Loading distribution from simulation (C_nM^2, harmonics 0-6/rev; white=0, black=0.24), condition as in Fig. 29

quality criteria as well.

- The application of the BVI analysis in the time domain to the simulated rotor blade loading, respectively to its nondimensional equivalent $C_nM^2(r,\psi)$, leads to results, which are comparable to the quality criterion from the blade pressure time histories in the flight tests. Although the curve of the phase sweep with the $2/rev$ IBC input of $\theta_2 = 1.0°$ from the simulation has a shift of $\Delta\phi_2 = 30°$ to the curve derived from the pressure histories, the essential features are similar.

- The reason for the noise reductions in the simulations at the phase angle $\phi_2 = 180°$ was found in an increase of the local downwash in the area around $\psi = 90°$ due to the $2/rev$ IBC input. This affects the vortices to be pushed to a lower flight

path within the rotor disk.

The presented analysis methods seem to be well suited for an approximate estimation of the radiated BVI noise emissions in flight. But as the analysis outputs, as well as the radiated noise, vary strongly with time, the quality criteria have to be averaged or low pass filtered in a suitable way, before they can be used for the application of a feedback signal for closed loop control.

References

[1] R. Kube, B.G. van der Wall, K.-J. Schultz, *Mechanisms of Vibration and BVI Noise Reduction by Higher Harmonic Control,* 20th European Rotorcraft Forum, Amsterdam, Netherlands, 1994

[2] W. R. Splettstößer et. al., *A Higher Harmonic Control Aeroacoustic Rotor Test (HART) -Test Documentation and Represantative Results-,* DLR IB129-95/28, Braunschweig, Germany, 1995

[3] D. Schimke et. al., *Individual Blade Control by Servo-Flap and Blade Root Control A Collaborative Research and Development Programme,* 23rd European Rotorcraft Forum, Dresden, Germany, 1997

[4] R. Kube et. al., *A Closed Loop Controler for BVI Impulsive Noise Reduction by Higher Harmonic Control,* 48th Annual Forum of the Helicopter Society, Washington DC, 1992

[5] W. R. Splettstoesser et. al., *Key Results from a Higher Harmonic Control Aeroacoustic Rotor Test (HART) in the German-Dutch Wind Tunnel,* 21st European Rotorcraft Forum, Saint-Petersburg, Russia, 1995

[6] K.-J. Schultz, D. Lohmann, J. A. Lieser, K. D. Pahlke, *Aeroacoustic Calculation of Helicopter Rotors at DLR,* AGARD Conference Proceedings No. 552, Berlin, Germany, October 1994

[7] W. R. Splettstößer et. al., *The Effect of Individual Blade Pitch Control on BVI Noise-Comparison of Flight Test and Simulation Results,* 24th European Rotorcraft Forum, Marseilles, France, 1998

[8] B.G. van der Wall *An Analytical Model of Unsteady Profile Aerodynamics and its Application to a Rotor Simulation Program,* 15^{th} European Rotorcraft Forum, Amsterdam, Netherlands, 1989

[9] B.G. van der Wall *Analytic Formulation of Unsteady Profile Aerodynamics and its Application to Simulation of Rotors,* DLR-FB 90-28, 1990, also: ESA-Report No. ESA-TT-1244, 1992

[10] P. Beaumier, J. Prieur, G. Rahier, P. Spiegel, A. Demargne (ONERA) C. Tung, J.M. Gallmann, Y.H. Yu (AFDD) R. Kube, B.G. van der Wall, K.J. Schultz, W.R. Splettstoesser (DLR) T.F. Brooks, C.L. Burley (NASA), D. D. Boyd (Lockheed) *Effect of Higher Harmonic Control on Helicopter Rotor Blade-Vortex Interaction Noise: Prediction and Initial Validation,* AGARD-CP-552, 1995 also: 75^{th} Fluid Dynamics Symposium, Berlin, Germany, 1994

[11] D. Petot, G. Arnaud, R. Harrison, J. Stevens, D. Teves, B.G. van der Wall, C. Young, E. Szchnyi, *Stall Effects and Blade Torsion - an Evaluation of Predictive Tools,* 23^{rd} European Rotorcraft Forum, Dresden, Germany, 1997

[12] U. Leiss *A Consistent Mathematical Model to Simulate Steady and Unsteady Rotor-Blade Aerodynamics,* 10^{th} European Rotorcraft Forum, Den Haag, Netherlands, 1984

[13] U. Leiss *Unsteady Sweep - A key to Simulation of Threedimensional Rotor Blade Airloads,* 11^{th} European Rotorcraft Forum, London, England, 1985

[14] B.G. van der Wall, J.G. Leishman *On the Influence of Time-Varying Flow Velocity on Unsteady Aerodynamics,* Journal of the American Helicopter Society, Vol. 39, Nr. 4, 1994

[15] K.W. Mangler, H.B. Squire *The induced velocity field of a rotor,* R & M 2642, 1950

[16] T.S. Beddoes *A Wake Model for High Resolution Airloads,* US Army/AHS International Conference on Rotorcraft Basic Research, Research Triangle Park, NC, 1985

[17] C. Goepel, B.G. van der Wall *Berechnung der induzierten Geschwindigkeiten des Rotorversuchsstandes ROTEST im DNW,* DLR IB 111-89/27, 1989

[18] B.G. van der Wall, M. Roth, *Free-Wake Analysis on Massively Parrallel Computers and Validation with HART Test Data,* 53^{rd} Annual Forum of the American Helicopter Society, Virginia Beach, VA, USA, 1997